JOURNAL OF CHEMICAL INFORMATION AND MODELING

Article

pubs.acs.org/jcim

A Contribution to the Drug Resistance Mechanism of Darunavir, Amprenavir, Indinavir, and Saquinavir Complexes with HIV-1 Protease Due to Flap Mutation I50V: A Systematic MM−PBSA and Thermodynamic Integration Study

Georgios Leonis,*[,†] Thomas Steinbrecher,[‡] and Manthos G. Papadopoulos*[,†]

[†]Institute of Biology, Medicinal Chemistry and Biotechnology, National Hellenic Research Foundation, 48 Vas. Constantinou Avenue, Athens 11635, Greece

[‡]Institute of Physical Chemistry, Department of Theoretical Chemical Biology, KIT, Kaiserstrasse 12, 76131 Karlsruhe, Germany

Supporting Information

ABSTRACT: The emergence of HIV-1 drug-resistant mutations is the major problem against AIDS treatment. We employed molecular dynamics (MD) calculations and free energy (MM−PBSA and thermodynamic integration) analyses on wild-type (WT) and mutated HIV-1 protease (HIV-1 PR) complexes with darunavir, amprenavir, indinavir, and saquinavir to clarify the mechanism of resistance due to the I50V flap mutation. Conformational analysis showed that the protease flaps are increasingly flexible in the I50V complexes. In the WT, stabilization of the HIV-1 PR structure is achieved via interflap and water-mediated hydrogen-bonding interactions between the flaps. Furthermore, hydrogen bonds between drugs and binding cavity residues (Asp29/29′/30/30′) are crucial for effective inhibition. All these interactions were significantly diminished (or absent) in the mutated forms, thus denoting their importance toward binding. Thermodynamic integration calculations reproduced the experimental data to within ≈1 kcal mol^{-1} and showed that the I50V mutation results in weaker binding free energies for all analyzed complexes with respect to the WT. It was observed that the loss in binding energy upon mutation was mostly enthalpically driven in all complexes, with the greatest effect coming from the reduction of van der Waals interactions. Our results motivated us to test two novel compounds that have been synthesized to maximize interactions with HIV-1 PR. MM−PBSA and TI calculations showed that compound **3c** (Ghosh et al. *Bioorg. Med. Chem. Lett.* **2012**, *22*, 2308) is a promising protease inhibitor, which presents very effective binding to the WT PR ($\Delta G_{MM-PBSA}$ = −17.2 kcal mol^{-1}, ΔG_{exp} = −16.1 kcal mol^{-1}). Upon I50V mutation, the complex binding free energy was weakened by a $\Delta\Delta G_{TI}$ of 1.8 kcal mol^{-1}, comparable to the marketed inhibitors. This predicts that I50V may confer low resistance to **3c**. This computational comparative study contributes toward elucidation of the I50V drug-resistance mechanism in HIV-1 PR.

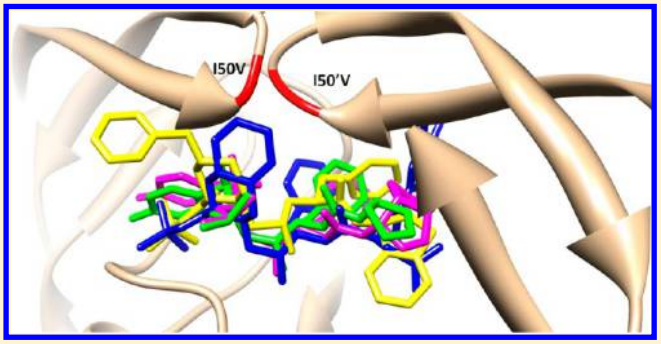

INTRODUCTION

The human immunodeficiency virus type 1 aspartic protease (HIV-1 PR) is considered a major target for anti-AIDS therapy,[1] since it modulates the lifecycle of HIV-1 by cleaving the Gag−Pol polypeptide to produce functional viral proteins.[2,3] The primary information on the HIV-1 PR crystal structures suggested that the enzyme possesses a symmetric, homodimeric structure and has an active site that is very similar to that of proteases belonging to the pepsin family.[4] The dimer interface includes the active site of the protease, which comprises two catalytic triplets (Asp−Thr−Gly) in positions 25/25′, 26/26′, and 27/27′.[5] In the outer part of the dimer, residues 43−58 (chain A) and 43′−58′ (chain B) belong to the flap region of the protease, and they form two β-hairpin structures that cover the active site. The two flaps have been implicated in the entrapment and binding of inhibitors to the protease.[6−8] While they appear significantly flexible in the apo (unbound) form of HIV-1 PR,[5,6,9] several theoretical and experimental studies have suggested that the flap region is considerably stabilized upon substrate binding, thus inducing a compact structure to the complex.[7,10]

The catalytic site is located at the bottom of a cavity, in a region whose structure is stabilized via multiple hydrogen bonds (HBs). The carboxylate groups of Asp25/25′ are almost coplanar and are found in close proximity to each other. The protonation state of the aspartic acid residues in the active site of HIV-1 PR has been a matter of debate in the last years; since it is generally accepted that an unprotonated active site is not associated with effective binding, the possibility of either a monoprotonated or a diprotonated active site is dominant.[11−15] In this study, the active site was considered monoprotonated

Received: April 7, 2013
Published: July 8, 2013

 © 2013 American Chemical Society dx.doi.org/10.1021/ci4002102 | J. Chem. Inf. Model. 2013, 53, 2141−2153

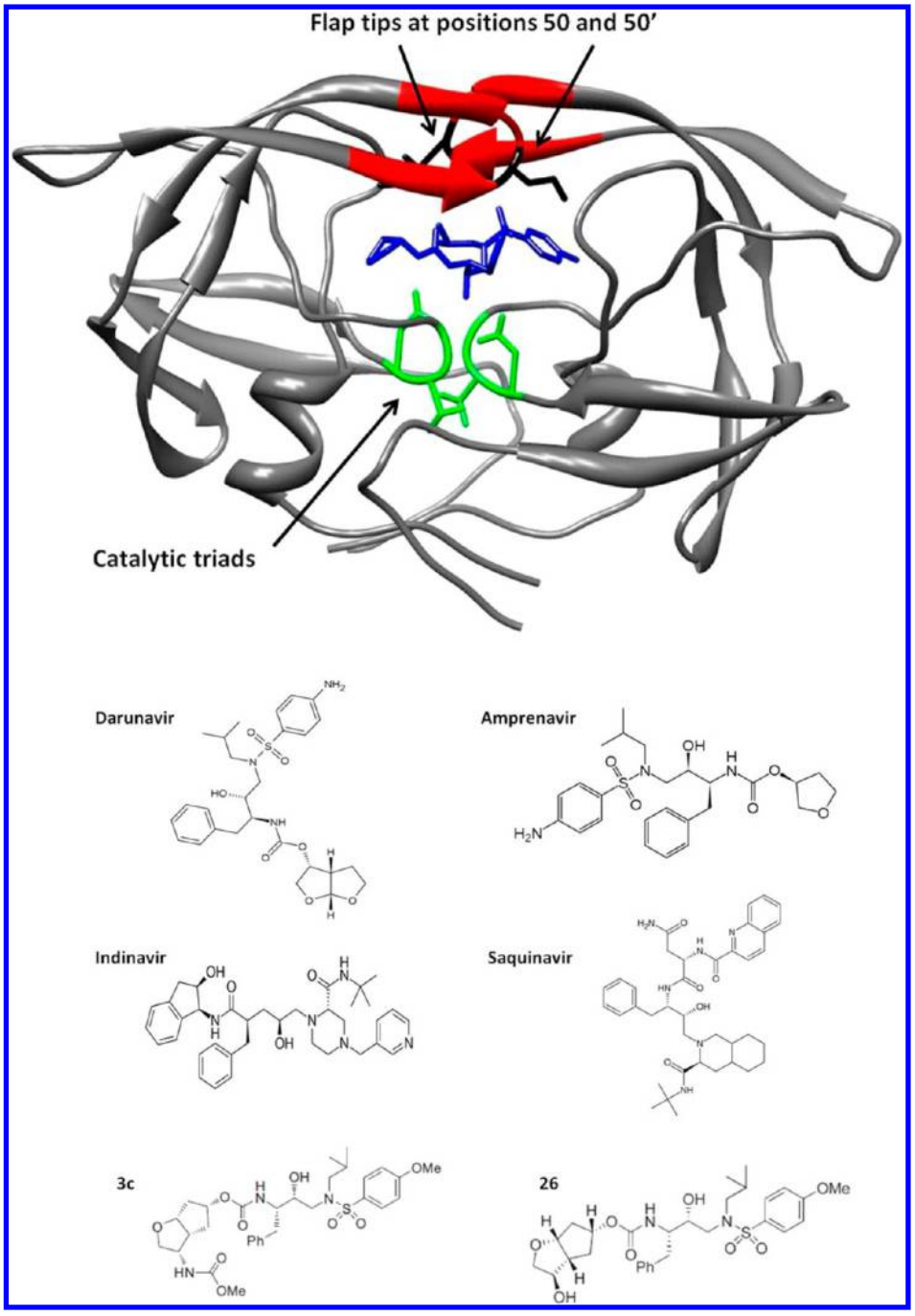

Figure 1. The structures of HIV-1 PR bound to the drug amprenavir and of the HIV-1 PR inhibitors used in this study; **3c**[30] and **26**[29] have been synthesized by Ghosh et al.

(on Asp25, chain A), according to previous experimental and theoretical evidence that supports this choice.[11,15]

It has been shown that the binding of a protease inhibitor (PI) into HIV-1 PR induces substantial structural changes to the protein.[16] Most of the HIV-1 PR inhibitors have been designed to develop hydrogen bonding (HB) interactions primarily with backbone atoms of the protease and are found in extended conformations at the active site of the enzyme.[16] Moreover, they present enhanced interactions with hydrophobic amino acids in the binding cavity.[17] Currently, nine PIs (indinavir, ritonavir, saquinavir, nelfinavir, amprenavir, lopinavir, atazanavir, tipranavir, and darunavir) have been approved by the U.S. Food and Drug Administration (FDA) and are available on the market.[16] Unfortunately, the emergence of drug-resistant viral strains reduces the susceptibilities to PIs and renders the highly active antiretroviral therapy (HAART)[18] eventually ineffective.[19] Resistance to PIs usually occurs after specific amino acid substitutions reduce the inhibitor's affinity to the mutant PR.[20,21] Extensive clinical studies have resulted in the identification of several mutations related to drug-resistant HIV-1 strains.[22] For example, it is known that mutations at approximately half of the total HIV-1 PR residues are related to one or more experimentally tested protease inhibitors and nearly a quarter of the total HIV-1 PR residues are involved in resistance against drugs that are currently used in patients.[23] Therefore, the investigation of conformational properties and

dx.doi.org/10.1021/ci4002102 | J. Chem. Inf. Model. 2013, 53, 2141−2153

binding patterns of PIs in HIV-1 PR complexes with mutations that are directly associated with resistance is critical for the development of improved medication.

In this study, we apply computational techniques [molecular docking, molecular dynamics (MD), molecular mechanics Poisson−Boltzmann surface area (MM−PBSA), and thermodynamic integration (TI) free energy methods] on HIV-1 PR crystallographic models, and in combination with experimental data, we systematically examine the effect of the I50V drug resistance−associated mutation. This mutation is of particular interest, since it confers resistance to most of the 9 drugs mentioned above, and it occurs in protease's flap region, which directly modulates the entrance of ligands into the binding site. Experimental evidence shows that the I50V mutation displays profound effects (related to a drug's binding affinity) in the cases of darunavir (DRV), amprenavir (APV), indinavir (IDV), and saquinavir (SQV).[22] Therefore, we have chosen these four inhibitors for MD and free-energy calculations into both wild-type (WT) and I50V-mutated forms of HIV-1 PR. Such an analysis, which is based on the comparison of structural and thermodynamic data to experimental results, allowed us to elucidate the influence of the I50V mutation on DRV, APV, IDV, and SQV protease recognition. The structure of WT HIV-1 PR bound to APV, and the chemical structures of the four drugs, are shown in Figure 1.

Many previous studies have conducted MD simulations on drug−HIV-1 PR complexes either in WT or in mutated forms.[14,24−27] However, the work presented here is the first to combine long MD simulations with both MM−PBSA and rigorous TI calculations for several inhibitors in active clinical use. Numerous crystal structures of HIV-1 PR, either in the apo form or bound to a variety of inhibitors have been deposited in the Protein Data Bank (PDB) over the years.[28] For consistency, all experimental evidence (PDB structures, conformational patterns, and inhibition assays) that is used in this article has been based on the results obtained from a single research group (I. T. Weber and co-workers). The aim of this study was to link the clinically-relevant drug-resistant mutation I50V with the binding and structural properties of HIV-1 PR inhibitors. Then, one may use this approach to predict the effects of the particular mutation in the presence of novel inhibitors. For this purpose, two promising compounds (**3c** and **26**, Figure 1)[29,30] have also been simulated in complexes with the WT and I50V forms of the protease, and their energetic profiles have been evaluated.

METHODS

Our methodology included (i) eight MD simulations for DRV−HIV-1 PR, APV−HIV-1 PR, IDV−HIV-1 PR, and SQV−HIV-1 PR in the WT and I50V forms of the protease to compare the conformational properties and dominant interactions between inhibitors and proteases, (ii) eight MM−PBSA calculations to estimate the binding affinities and to decompose them into contributions from different types of interactions, (iii) four TI calculations for the WT−I50V pairs of each drug to further validate our results, (iv) MD simulations of apo HIV-1 PR to compare the behavior of the complexes to the unbound protease, and (v) docking, MM−PBSA, and TI calculations for the WT and I50V complexes of HIV-1 PR with two additional compounds (**3c** and **26**) to test their effectiveness as new potent protease inhibitors. **3c** and **26** have been designed, synthesized, and biologically evaluated, as well as their crystal structures have been solved in complexes with HIV-1 PR by A. K. Ghosh and co-workers; for consistency with their published results, we have kept the naming of compounds **3c** and **26** intact.

Molecular Dynamics Simulations. The crystal structures of drug−HIV-1 PR (drug = DRV, APV, IDV, SQV, **3c**, **26**) as obtained from the PDB were used for MD calculations. Initial coordinates for each WT complex correspond to the following PDB codes: DRV-PR, 2IEN;[31] APV-PR, 3NU3;[32] IDV-PR, 1SDT;[33,34] SQV-PR, 3OXC;[35] **3c**-PR, 4DFG;[30] and **26**-PR, 3ST5.[29] All-atom, unrestrained MD simulations in explicit solvent have been carried out for each protein complex (WT and I50V) using the SANDER program of AMBER 11.[36−38] Crystal water molecules were retained in the structures before adding missing hydrogen atoms with the tLEaP module of AMBER. tLEaP was also used to construct the mutated PR structures. Atomic partial charges, bond lengths, bond angles, dihedral angles, force constants, and van der Waals parameters for HIV-1 PR were represented by the AMBER ff99SB force field.[39] Force field parameters and partial charges for each drug were assigned as follows: missing hydrogen atoms were added with the program reduce.[40] Next, the geometry of the drugs was optimized with Gaussian 09,[41] using the HF/6-31G* basis set. Finally, the ANTECHAMBER module was used to derive the RESP atomic partial charges for each drug, and the general AMBER GAFF force field was employed to obtain the force field parameters.[42] Each system was neutralized with tLEaP by adding 7 Cl^- counterions and it was solvated with approximately 9500 water molecules. Explicit solvation has been represented by the TIP3P water model[43] in truncated octahedral periodic boundary conditions, with a cutoff distance of 10 Å. Long-range electrostatic interactions have been calculated using the particle mesh Ewald (PME) method.[44] A four-step, extensive energy minimization process with the steepest descent method (followed by the conjugate gradient algorithm) was used to relieve unwanted steric interactions and to direct the systems toward energetically favorable conformations. During the first step, the solute (drug−HIV-1 complex) was kept almost fixed with a harmonic force constant of 500 kcal mol^{-1} $Å^{-2}$, while the water molecules were allowed to relax. Next, the strength of the restraint was gradually reduced in two steps from 10 to 2 kcal mol^{-1} $Å^{-2}$. Finally, the restraint was removed, to allow all atoms to move freely. Each of the four steps was realized in 5000 cycles with a cutoff of 20 Å. After minimization, a gentle heating of the system under constant volume was performed, over 100 ps with the gradual increase of the temperature from 0 to 300 K. The SHAKE algorithm[45] was applied to constrain all bond lengths involving hydrogen to their equilibrium distance, and a 2 fs time step was used. The Langevin thermostat[46] with a collision frequency of 2.0 ps^{-1} was used for temperature control. A restraint of 10 kcal mol^{-1} $Å^{-2}$ was applied to the solute. The same restraint was kept for the next 100 ps of equilibration in the NPT ensemble. A final equilibration stage of 100 ps was performed with all atoms of the system unrestrained. Subsequent unrestrained MD simulations in the NPT ensemble lasted for 20 ns. The SHAKE algorithm and Langevin thermostat, along with a 10 Å nonbonded cutoff, were applied during the heating, equilibration, and production MD periods. Further analysis (RMSD, atomic fluctuations, distances, angles, and HB calculations) was performed on the resulting trajectories with the ptraj module of AMBER. Cutoffs of 3.5 Å for the donor−acceptor distance and of 120° for the donor−hydrogen−acceptor angle have been used to define HB interactions. Clustering calculations have

been carried out with MOIL-View 10.0, based on the hierarchical algorithm.[47] An RMSD cutoff of 1.0 Å was introduced to classify 2000 conformations into individual clusters.

MM−PBSA Calculations. MM−PBSA is an end point method that involves calculations of free-energy differences between two states.[48−52] The partition of the binding free energy into contributions allows for a valuable insight into the complex process of association. For each inhibitor-protein system, the binding free energy change (ΔG_{bind}) accompanies the binding process:

$$\text{Protein} + \text{Inhibitor} \rightarrow \text{Complex}$$

The procedure was applied by considering 2000 snapshots of the complexes that did not contain any water molecules or counterions. To obtain a low statistical error, snapshots were equally spaced at 10 ps intervals, thus ensuring that structures are uncorrelated.[49] For every snapshot, the binding free energy for each complex is calculated using the following equation:

$$\Delta G_{bind} = G_{complex} - (G_{protein} + G_{inhibitor}) \quad (1)$$

where ΔG_{bind} is the total binding free energy, $G_{complex}$, $G_{protein}$, and $G_{inhibitor}$ are the energies for the complex, the protein (HIV-1 PR), and the inhibitor (DRV, APV, IDV, SQV, **3c**, **26**), respectively. The binding energy can also be expressed as a combination of enthalpic and entropic contributions:

$$\Delta G_{bind} = \Delta H - T\Delta S \quad (2)$$

The enthalpy of binding is given by

$$\Delta H = \Delta E_{MM} + \Delta G_{sol} \quad (3)$$

where ΔE_{MM} defines the interaction energy between the protein and the inhibitor computed with the molecular mechanics method, and ΔG_{sol} is the change in solvation free energy upon ligand binding.

ΔE_{MM} is further divided into

$$\Delta E_{MM} = \Delta E_{elec} + \Delta E_{vdW} \quad (4)$$

ΔE_{elec} is the electrostatic interaction energy and ΔE_{vdW} is the van der Waals interaction energy. For the calculation of these two terms, no cutoff point was applied. Furthermore, the solvation energy (eq 3) is defined by the combination of electrostatic (ΔG_{PB}) and nonpolar (ΔG_{NP}) contributions:

$$\Delta G_{sol} = \Delta G_{PB} + \Delta G_{NP} \quad (5)$$

The electrostatic (ΔG_{PB}) energy is approximated by the Poisson−Boltzmann (PB) method[53] using the PBSA module of AMBER, and the hydrophobic contribution to solvation (ΔG_{NP}) is determined via calculation of the solvent-accessible surface area (SASA):

$$\Delta G_{NP} = \gamma^{*}\text{SASA} + \beta \quad (6)$$

For the surface tension (γ) and for the offset (β), we have considered the standard values of 0.005420 kcal mol^{-1} Å^{-2} and −1.008000 kcal mol^{-1}, respectively. ΔG_{NP} was computed via eq 6, with the linear combinations of pairwise overlaps (LCPO) method.[54] A probe radius of 1.4 Å for the solvent has also been used in the SASA calculation.

Following recent studies on the optimal performance of MM−PBSA for hydrophobic systems, the values for the dielectric constant of the solvent and the solute were set to 80.0 and 1.0, respectively.[55] The finite-difference grid spacing was set to 0.5 Å, and the ratio between the longest dimension of the grid and that of the solute was 4.0. The ionic strength was set to 0.1 M. The entropic contribution (eq 2) was calculated using the nmode module of AMBER, over 200 snapshots to save computational time. Instead of modeling the water environment by explicit simulations, MM−PBSA discards the water molecules and uses a parametrized implicit water model (PB). Sometimes, this may be a disadvantage that accounts for differences between predictions and experimental results. However, the LCPO method for estimating the hydrophobic contribution shows sufficient performance even for hydrophobic systems, such as the binding cavities of HIV-1 PR and renin, satisfactorily reproducing the experimental results. The performance of MM−PBSA has been recently evaluated.[55] Six different protein systems have been tested as substrates for 59 ligands. Various factors, such as the length of the MD simulation and the values of the solute dielectric constant have been considered to affect the quality of the results. Particularly, the importance of the conformational entropy was emphasized, as well as the adequacy of MM−PBSA to reliably calculate binding free energies.

Thermodynamic Integration Calculations. Calculating the binding energy (ΔG) in protein complexes offers insights into the binding mechanism. However, the most important information when comparing complexes, such as WT and mutant proteases, comes from the relative difference ($\Delta\Delta G$) between the two states. TI is a technique that calculates the relative energy difference from MD or Monte Carlo (MC) simulations and is based on the following scheme:[56,57]

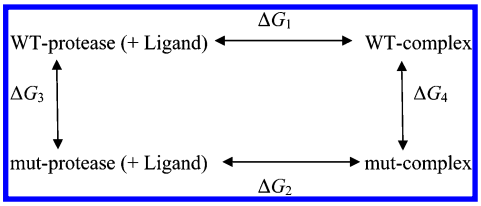

where

$$\Delta\Delta G = \Delta G_2 - \Delta G_1 = \Delta G_4 - \Delta G_3 \quad (7)$$

ΔG_1 and ΔG_2 represent the binding of a ligand to two different proteins (WT and mutated forms), while ΔG_3 and ΔG_4 represent "alchemical" transformations of the potential energy function along a nonphysical, virtual coordinate λ, corresponding to a change from one protein to the other either when solvated only in water (ΔG_3) or when bound to a ligand (ΔG_4).

The TI method calculates the binding free energy based on the following equation:

$$\Delta G^0 = \int_0^1 \left\langle \frac{\partial V(\lambda)}{\partial \lambda} \right\rangle_\lambda d\lambda \quad (8)$$

where angular brackets represent a Boltzmann-weighted average and with the integral typically solved numerically using several simulations at fixed λ values:

$$\Delta G = \sum_{i=1}^{n} W_i \left\langle \frac{\partial V}{\partial \lambda} \right\rangle_{\lambda_i} \quad (9)$$

where λ is the coupling parameter and V denotes the λ-coupling potential function. The values for λ and their respective weights (W_i) are assigned based on the Gaussian quadratic formula. For $\lambda = 0$, the $V(0)$ potential function corresponds to the WT, and for $\lambda = 1$, the $V(1)$ potential

dx.doi.org/10.1021/ci4002102 | J. Chem. Inf. Model. 2013, 53, 2141−2153

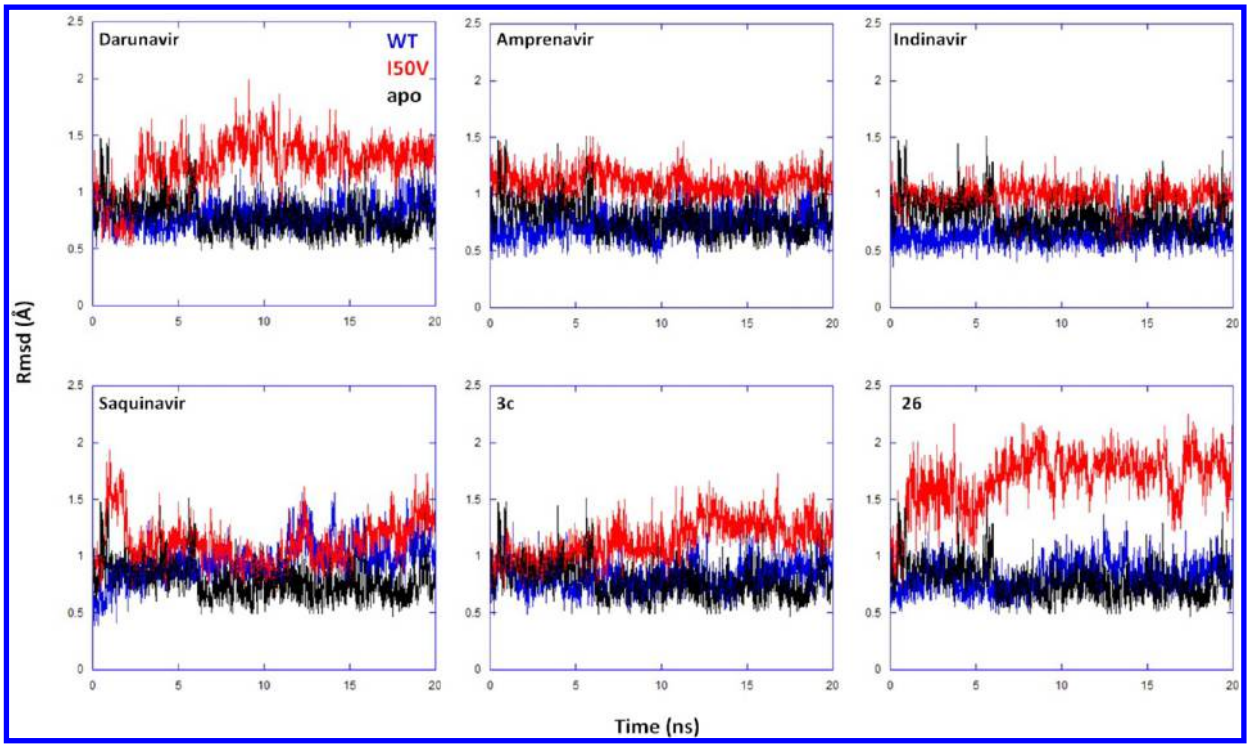

Figure 2. RMSD for Cα atoms of HIV-1 PR flaps in drug-bound WT forms (blue), drug-bound I50V forms (red), and unbound (apo) form (black).

function corresponds to the single mutant I50V. The TI procedure was realized for each λ in three steps: (a) charge removal from the side chain (Cδ, Hδ1, Hδ2, and Hδ3) atoms of Ile, (b) changing Ile into Val, and (c) charge addition on the side chain hydrogen atom Hγ1 of Val (see Figure S1 of the Supporting Information). Since the WT and mutant enzymes have a different number of atoms due to the change in position 50, we used soft-core potentials that were activated only during the second step, which involves the disappearance and appearance of atoms. The atoms involving the TI transformation Ile → Val are shown in Figure S1 of the Supporting Information. MD simulations for the TI calculation were performed according to the protocol described above. The sampling space was defined by 12 different λ values, and for each λ, we ran six (3 steps for each WT and I50V) independent, 2 ns MD simulations (1 ns for the **3c** complex only). For our calculations, the values of λ and their respective weights were taken from the AMBER 11 manual (Table S1 of the Supporting Information).

RESULTS AND DISCUSSION

Conformational Properties of Drug−HIV-1 PR Complexes in WT and I50V Forms. MD simulations for the eight drug complexes (and the apo HIV-1 PR) were initiated with the closed forms of their crystal structures as described in Methods. All simulations converged after the first 5 ns with respect to protein structural changes, thus denoting the early stabilization of the systems. Cα-based RMSD calculations with respect to the crystal structure for each complex showed that proteases' structures fluctuate slightly around average values, which are lower than 1.7 Å (Figure S2 of the Supporting Information). The apo form of HIV-1 PR also showed minor structural changes during the simulations; it is, however, noted that unbound forms of the protease are potentially unstable, since their flaps alternate among closed, open, and semiopen states. Ultimately, this confers flexibility to the overall structure of the protease as observed in a previous study involving a lengthier simulation of unbound HIV-1 PR.[58] The mutated form of HIV-1 PR appeared less stable with more significant structural changes compared to the WT when bound to darunavir. Darunavir−(WT)HIV-1 PR was particularly stable, with an average RMSD ≈ 1.1 Å, but in the (I50V)HIV-1 PR complex, the drug induced instability to the protease, as reflected by the higher RMSD values (up to 1.7 Å). This implies that the flap mutation may have induced structural rearrangements to the complex, possibly leading to resistance. Indinavir and saquinavir-bound proteases were slightly more stable than darunavir−HIV-1 PR complexes. This is in agreement with earlier experimental observations, suggesting that both WT and I50V forms do not present major structural changes when associated with saquinavir.[35] Indinavir−HIV-1 PR was particularly stable in both forms of the protease, with an average RMSD < 1 Å. The mobility of each drug into HIV-1 PR was also studied (Figure S3 of the Supporting Information): in general, all drugs appear relatively stable in both forms of the protease, except saquinavir that underwent structural changes into the cavity of WT HIV-1 PR as denoted by its RMS deviations, which range between 0.5 and 2 Å. Initially, saquinavir bound to the WT protease was very stable, being practically unchangeable inside the cleft for the first 5 ns of the simulation. Next, it followed a noticeable shift at 5−6 ns that lasted for 4 ns, and then another conformational change during 10−13 ns, before stabilizing for the remaining of the simulation. Elucidation of main interactions (especially possible rearrangement in hydrogen bonds) into the binding cavity for the drug may shed light on this observation. Similar interactions may also be responsible for sudden shifts of indinavir when bound to WT protease at 4, 10, and 17.5 ns. In the mutated form, indinavir also displayed changes at 4.5, 10, and 15 ns.

dx.doi.org/10.1021/ci4002102 | J. Chem. Inf. Model. 2013, 53, 2141−2153

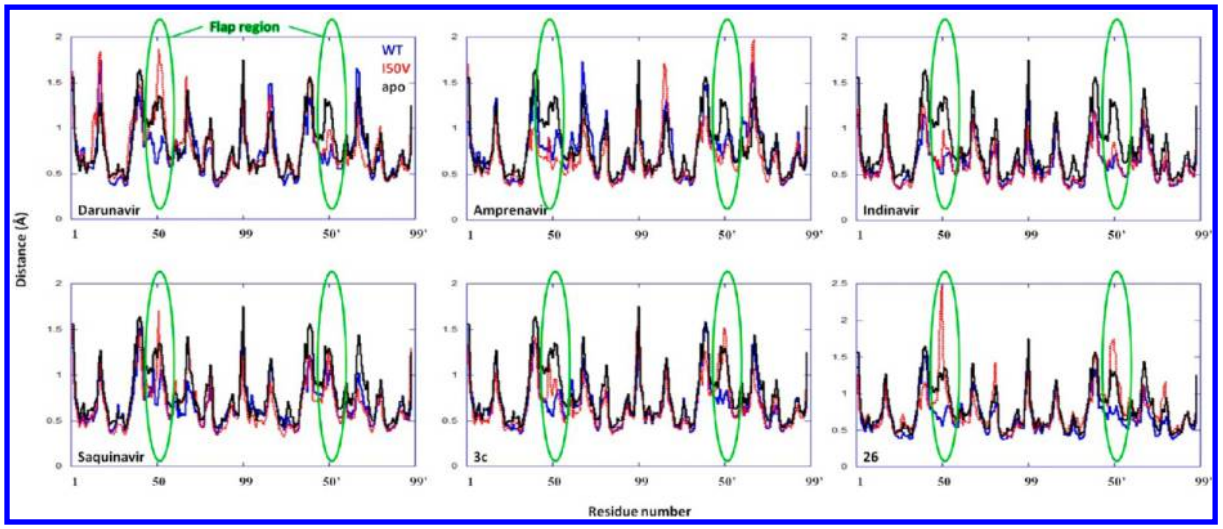

Figure 3. Cα atomic fluctuations of HIV-1 PR in its drug-bound WT forms (blue), drug-bound I50V forms (red), and unbound form (black).

Binding of an effective inhibitor into HIV-1 PR is usually accompanied by closure of the flaps that results in a stable protease structure. A reasonable way to describe the extent of the flap opening is to measure the distance between flap tips (Ile/Val50–Ile/Val50′). In WT and I50V darunavir complexes, the flap distance remains stable at 5–6 Å throughout the simulation, thus inducing a compact structure to the protease (Figure S4 of the Supporting Information); indinavir and amprenavir complexes showed analogous behavior (in both WT and mutated forms), thus suggesting that the mutation did not directly affect the conformation of the flaps. In accordance with a previous study, entrapment of a substrate into the cavity of HIV-1 PR may induce a tight approach of the flaps, but this property alone is not sufficient for effective binding.[58] Finally, although a similar observation is valid for the saquinavir complexes, the flap distance in I50V HIV-1 PR appears more variable, ranging from 7 to 8.4 Å, with an average of ∼7.5 Å, and the flap distance in WT fluctuates between 4.5 and 7.5 Å. As noted above, saquinavir was relatively mobile in the WT form of HIV-1 PR (Figure S3 of the Supporting Information). This structural flexibility of the drug may stem from the absence of permanent interactions between saquinavir and binding cavity residues of the protease that in turn may induce a larger flap separation compared to the I50V.

HIV-1 PR Flaps Dynamics. Calculations have also been carried out for the flaps [RMSD on Cα of residues 43–58 (chain A) and 43′–58′ (chain B)] of both forms of the protease, starting from each closed state and overlapping on the same state. RMS values for all drug–bound WT forms of the protease were very low and similar to the values calculated for the apo HIV-1 PR (average deviation 0.8 Å), meaning that HIV-1 PR is found mainly in its closed state (Figure 2). The flaps in the WT saquinavir-bound HIV-1 PR were slightly more flexible, with RMSD values reaching up to 1.4 Å. This is indicative of a less compact structure of the protease; however, even in this case, the flaps remain predominantly closed on top of saquinavir. Similarly, RMSDs for the flaps of the mutated forms of HIV-1 PR appear higher than the corresponding WT proteases. In a recent study, however, it has been suggested that entrapment of a ligand after flap closure may occur regardless of its inhibitory potency against HIV-1 PR.[58] This denotes that a "closed" protease structure does not necessarily implicate effective inhibitor binding.

Structural Flexibility of HIV-1 PR. While the structures of the complexes remained stable overall, certain regions of the protease may present differences in flexibility. Cα atomic fluctuation calculations for each residue of HIV-1 PR revealed that residues such as the catalytic Asp25/25′ present a high degree of stability in all WT and I50V forms (Figure 3). Importantly, it was observed that flap residues in the mutated form of HIV-1 PR when bound to each drug showed an increased mobility compared to the flaps in the WT form of the protease. The WT flaps appear particularly stable in all drug-bound complexes, whereas the flaps in the I50V forms fluctuate significantly more, with the only exception of amprenavir complexes that are equally stable in both WT and I50V forms. In a recent study from our group involving saquinavir complexes in WT and 7 singly mutated forms of HIV-1 PR, it was concluded that specific mutations, which increase the flexibility of the flaps, diminish binding significantly.[59] In agreement with our observations, Shen et al. attributed the reduced efficacy of amprenavir against (I50V)HIV-1 PR to the conformational rearrangements observed between the WT and mutated forms of the bound protease.[32]

Clustering Analysis. Clustering calculations in all HIV-1 PR complexes have been performed to identify possible conformational changes on the drugs due to I50V mutation. As shown above, it was concluded that inhibitors in either WT or mutated forms of the protease appear quite stable during the simulation. In particular, darunavir in WT HIV-1 PR has one principal conformation, while in the I50V mutant, it adopts a major configuration (being present for 82% of the simulation time), which differs from a less populated structure (14%) only in the orientation of the *bis*-THF moiety (Figure S5 of the Supporting Information). Similarly, amprenavir and saquinavir in WT and I50V forms of the protease showed very stable conformations, which slightly differ in the flexibility of groups, such as tetrahydrofuranyl and isobutyl (amprenavir), and phenyl and carbamoyl (saquinavir). The increased flexibility of saquinavir into WT HIV-1 PR observed above may well be explained by the mobility of phenyl and carbamoyl groups. However, the clustering analysis showed that despite this, saquinavir acquires primarily one (overall stable) conformation into each form of the protease. Indinavir presented very minor conformational changes, having a practically unchanging structure in both forms of the protease. A minor cluster (5%)

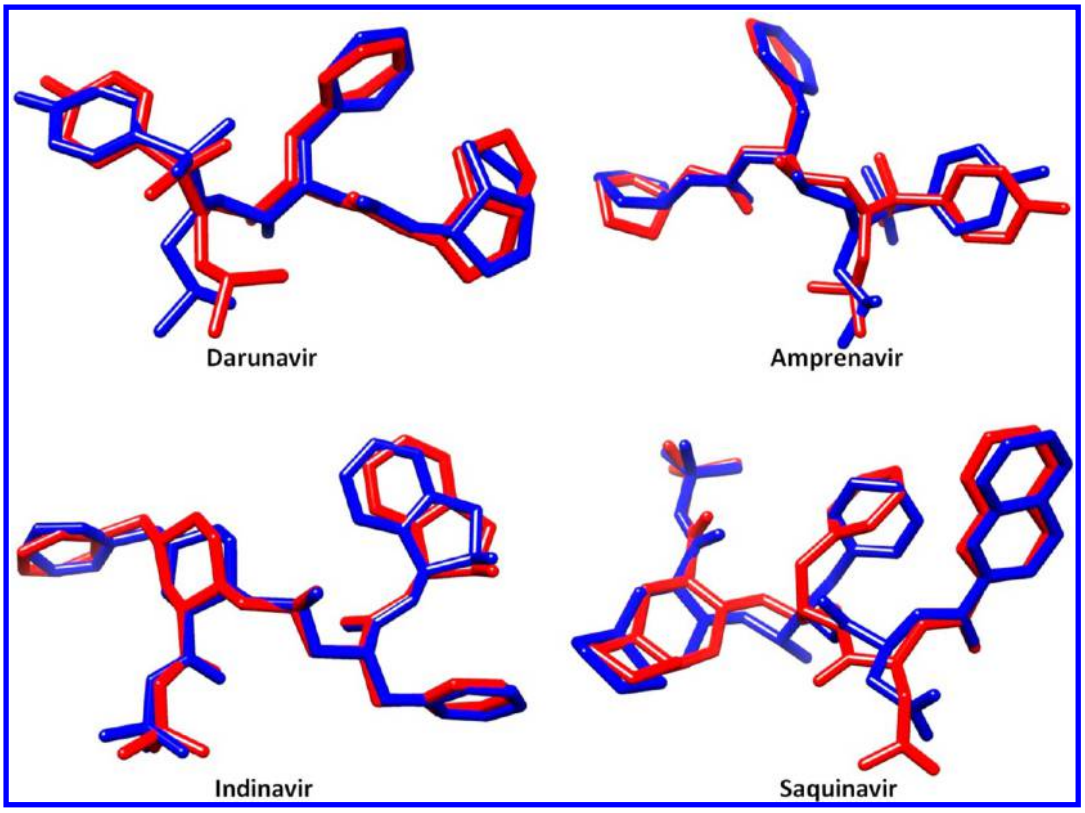

Figure 4. Comparison of representative structures of darunavir, amprenavir, indinavir and saquinavir into WT (red) and I50V (blue) forms of HIV-1 PR.

Table 1. Main HB Interactions Involving the Flaps of Inhibitor-Bound HIV-1 PR

interaction	occurrence[b]									
	DRV–PR		APV–PR		IDV–PR		SQV–PR		**3c**–PR	
acceptor flap–donor flap[a]	WT	I50V	WT	I50V	WT	I50V	WT	I50V	WT	I50V
Ile/Val50′ O–Gly51 N–H	91	85	92	98	89			84	89	
Ile/Val50′ O–Gly52 N–H	17	17	23		32			32	10	
Ile/Val50′ O–Gly49 N–H							18			32
water-mediated HB										
Ile/Val50–H_2O–Ile/Val50′	81	97	88	90	86	18	29		74	
Gly51–H_2O–Gly49′[c]							31			

[a]N and O refer to backbone nitrogen atoms and carbonyl oxygen atoms, respectively. [b]Occurrence is defined as the percentage of simulation time that a specific interaction exists; interactions occurring less than 10% of the simulation are not shown. [c]This interaction involves two water molecules. For a detailed description of flap HB interactions in each complex, see Tables S2–S7.

showed indinavir in the mutated HIV-1 PR to be slightly tilted compared to its most probable, extended conformation (Figure S5 of the Supporting Information).

Even though a high degree of structural stability was also observed in the other drugs, certain conformational changes may partially explain differences in binding between WT and mutated complexes. Comparison of the representative structures of each drug in WT and I50V proteases is given in Figure 4. As mentioned above, indinavir acquired almost identical conformations in both complexes, thus being practically unaffected by the mutation. Amprenavir appeared also relatively stable upon mutation; however, changes in the conformation of the tetrahydrofuranyl group, as well as differences in the flexibility of the isobutyl group, may be significant toward effective binding. Similarly, saquinavir presented minor differences in the orientations of the phenyl and carbamoyl groups between WT and I50V HIV-1 PR.

Hydrogen Bonding Interactions. Hydrogen-bonding analysis on the flap region (residues 47–54 and 47′–54′) of the WT protease complexes revealed the existence of 2 or 3 permanent HB interactions between backbone [Ile50′] and [Gly51, Gly52, Gly49] residues, which stabilized the flaps above each drug (Table 1 and Tables S2–S5 of the Supporting Information). Mutated proteases presented less frequent HB interactions between flaps with the exception of saquinavir-bound (I50V)HIV-1 PR, whose flaps are bridged through more HBs than the WT form. Of particular importance was the identification of a water-mediated interaction between the two flaps of the WT protease when bound to each drug. It has been suggested that a water molecule contributes significantly toward efficient binding by bridging the two flaps together.[58] The structure of the flaps is mostly affected due to the mutation, and it was shown that the flap tips in WT forms are stabilized via interflap hydrogen bonds and water-mediated interactions.

dx.doi.org/10.1021/ci4002102 | J. Chem. Inf. Model. 2013, 53, 2141–2153

Table 2. Main HB Interactions between Inhibitors and HIV-1 PR in WT and I50V Forms

drug interaction	occurrence[b]									
	DRV–PR		APV–PR		IDV–PR		SQV–PR		3c–PR	
HIV-1 PR residue[a]	WT	I50V	WT	I50V	WT	I50V	WT	I50V	WT	I50V
Asp25′ OD2	100	21	100	98	58	100	100	100	86	100
Asp25′ OD1		79	42	51	97	63	13	10	17	23
Asp30 N–H	91	54	74	71			34		14	
Asp30 O	91	57	79	69			32			
Asp29′ N–H	87	13	19	42	93	82			12	50
Asp29′ OD1/OD2[c]					64	61				
Asp29 N–H	20		13	17			33	18	96	
Asp30′ N–H	81	11	17	39					27	
Gly27′ O			9	25	43	48	14			
Asp25 OD2-HD2			97	100	95	100	49	93	20	97
Gly48 O							82	90	83	
water-mediated HB										
apv/sqv–H_2O–Asp29′[d]			6	18			93	72		
idv–H_2O–Asp29[d]					75	70				
apv–H_2O–Arg87′[d]			18							

[a]N and O refer to backbone nitrogen atoms and carbonyl oxygen atoms, respectively. OD1 and OD2 refer to side chain carboxyl oxygen atoms. [b]Occurrence is defined as the percentage of simulation time that a specific interaction exists; interactions occurring in less than 5% of the simulation are not shown. [c]Indinavir interacts with either OD1 or OD2. [d]This interaction involves several water molecules. For a detailed description of HB interactions in each complex, see Tables S8–S13.

These interactions were significantly reduced upon mutation. Moreover, the role of the flap–flap interactions is also particularly important regarding dimer stabilization: indeed, Liu et al. suggested that dimer dissociation is favored in the case of the indinavir–(I50V)HIV-1 PR complex, due to the reduced intersubunit contacts between the flaps of the protease.[34]

The HB analysis between drug molecules and binding-cavity residues of HIV-1 PR revealed that multiple interactions stabilize the inhibitor–protease structures in both the WT and mutated forms. In particular, each drug is involved in several HBs with the protease's catalytic site, mostly with residues Asp25′, Asp29/29′, and Asp30 (Table 2 and Tables S8–S11 of the Supporting Information). Interactions between the side chain of Asp25′ and the drugs, as well as between the backbone of Asp29/29′ and the drugs, were observed in every complex. The backbone of Asp30 is also involved in significant HBs with all drugs except IDV, which interacts mostly with side chain atoms of Asp29′. Another interaction with the backbone of Gly27′ appears mainly in APV and IDV complexes. Interestingly, the I50V flap mutation induced the HB formation between Val50 of the mutated protease and the drugs (most notably darunavir). This was probably the main reason for the closed structure of the flaps in the mutated forms. In the case of SQV-bound (I50V)HIV-1 PR, stabilization of the flaps was also obtained, as we observed similar interactions that involve the drug and flap residue Gly48 (instead of Val50).

In general, it was noticed that in all complexes the number and frequency of HB interactions were diminished upon I50V mutation. Of particular interest was the observation that water mediated an interaction between SQV and Asp29′ in the WT form of HIV-1 PR. It was suggested that alternating water molecules formed a permanent bridge between the drug and the active site of the protease. A similar interaction involving water molecules and Asp29 was also observed in both the WT and mutated forms of IDV complexes. In the aforementioned study involving SQV complexes in different mutated forms, it was shown that the preservation of HBs of the drug with both the active site and flap residues in the WT and certain single mutants is also crucial for effective inhibition. Mutations that confer major resistance, such as G48V, L63P, and I84V did not present these (active site and flap) interactions.[59]

Figure 5 shows the HB interactions that are mostly affected by the I50V mutation. Drug-related HBs involving residues Asp30/30′ and Asp29/29′ were generally reduced in the mutated complexes. Interflap HBs and water-mediated (flap–flap and drug-active site) interactions were also diminished in the mutated complexes.

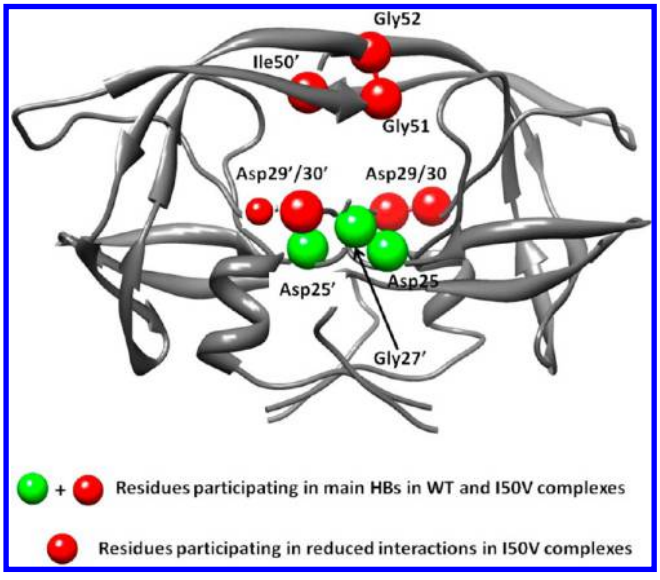

Figure 5. The diminishing of HB interactions in the HIV-1 PR binding cavity upon I50V mutation: an extended network involving the inhibitor and PR residues (in the active site and flaps, represented as spheres) stabilize the WT complexes into compact structures (red and green); I50V-mutated complexes retain only interactions involving certain active site residues (green).

dx.doi.org/10.1021/ci4002102 | J. Chem. Inf. Model. 2013, 53, 2141–2153

Table 3. Energetic Analysis for Drug−HIV1-PR Complexes As Obtained by MM−PBSA and TI Calculations

	Darunavir−HIV-1 PR		Amprenavir−HIV-1 PR		Indinavir−HIV-1 PR		Saquinavir−HIV-1 PR	
Energy[a] (kcal mol^{-1})	WT	I50V	WT	I50V	WT	I50V	WT	I50V
ΔE_{vdW}	−66.37 ± 0.07	−65.04 ± 0.08	−61.99 ± 0.09	−60.48 ± 0.09	−76.40 ± 0.08	−72.57 ± 0.09	−72.31 ± 0.11	−68.40 ± 0.10
ΔE_{elec}	−41.82 ± 0.11	−41.03 ± 0.15	−50.12 ± 0.13	−53.41 ± 0.12	−44.09 ± 0.12	−42.32 ± 0.13	−36.93 ± 0.21	−37.72 ± 0.15
$\Delta E_{MM,\ gas}$	−108.18 ± 0.11	−106.06 ± 0.14	−112.12 ± 0.14	−113.88 ± 0.15	−120.49 ± 0.12	−114.89 ± 0.14	−109.24 ± 0.21	−106.13 ± 0.18
ΔG_{PB}	73.05 ± 0.09	74.83 ± 0.13	72.47 ± 0.10	75.94 ± 0.11	82.22 ± 0.10	83.70 ± 0.11	72.03 ± 0.18	71.38 ± 0.14
ΔG_{NP}	−5.07 ± 0.01	−5.27 ± 0.01	−5.24 ± 0.01	−5.29 ± 0.01	−6.29 ± 0.01	−6.24 ± 0.01	−6.37 ± 0.01	−6.45 ± 0.01
ΔG_{solv}	67.98 ± 0.08	69.56 ± 0.12	67.23 ± 0.10	70.65 ± 0.11	75.93 ± 0.10	77.46 ± 0.11	65.66 ± 0.18	64.92 ± 0.14
$\Delta H_{(MM+solv)}$	−40.20 ± 0.09	−36.51 ± 0.11	−44.88 ± 0.10	−43.24 ± 0.11	−44.56 ± 0.11	−37.44 ± 0.12	−43.58 ± 0.14	−41.20 ± 0.12
$-T\Delta S_{tot}$	27.39 ± 0.38	28.51 ± 0.51	26.71 ± 0.40	26.21 ± 0.54	27.55 ± 0.52	31.60 ± 0.55	29.87 ± 0.44	30.33 ± 0.61
$\Delta G_{MM-PBSA}$	−12.81 ± 0.39	−7.99 ± 0.52	−18.18 ± 0.41	−17.03 ± 0.55	−17.01 ± 0.53	−5.84 ± 0.56	−13.71 ± 0.46	−10.87 ± 0.62
$\Delta\Delta G_{MM-PBSA}$	4.82		1.15		11.23		2.84	
K_i (nM)[b]	0.46	1509.41	0.000057	0.00039	0.00040	55617	0.10	12.04
$\Delta\Delta G_{TI}$[c]	0.657 ± 5.606		1.369 ± 5.487		1.354 ± 5.657		1.524 ± 5.964	
ΔG_{exp}	−12.68	−10.63	−13.49	−11.46	−12.72	−10.39	−12.87	−10.98
$\Delta\Delta G_{exp}$	2.05		2.03		2.33		1.89	
$K_{i\ exp}$ (nM)[d]	0.58 ± 0.10	18 ± 1	0.15 ± 0.04	4.5 ± 0.6	0.54	27.0	0.42 ± 0.07	10 ± 1

[a]Errors represent standard errors of mean: SEM = standard deviation/$N^{1/2}$, where N is the number of trajectory snapshots used in MM−PBSA calculations (N = 200 for entropy/$\Delta G_{MM-PBSA}$ calculations, and N = 2000 for everything else). [b]The K_i values were calculated with the equation $\Delta G = RT \ln K_i$ at 300 K. [c]Standard deviations in TI calculations represent the RMS values for each final result. [d]Experimental K_i values have been taken from references: [62] (DRV and SQV complexes), 20 (APV complexes), and 21b (IDV complexes).

dx.doi.org/10.1021/ci400210z | J. Chem. Inf. Model. 2013, 53, 2141−2153

Table 4. Energetic Analysis for HIV1-PR Complexes with Compounds 3c and 26, as Obtained by MM−PBSA and TI Calculations

	26−HIV-1 PR		3c−HIV-1 PR	
energy (kcal mol^{-1})	WT	I50V	WT	I50V
ΔE_{vdW}	−67.74 ± 0.08	−51.88 ± 0.12	−71.80 ± 0.08	−66.23 ± 0.11
ΔE_{elec}	−41.61 ± 0.21	−28.73 ± 0.18	−43.19 ± 0.20	−36.94 ± 0.15
$\Delta E_{MM,\ gas}$	−109.24 ± 0.21	−80.61 ± 0.20	−114.98 ± 0.19	−103.16 ± 0.19
ΔG_{PB}	71.33 ± 0.15	58.69 ± 0.16	74.58 ± 0.15	66.12 ± 0.15
ΔG_{NP}	−5.44 ± 0.01	−4.84 ± 0.01	−5.74 ± 0.01	−5.73 ± 0.01
ΔG_{solv}	65.89 ± 0.15	53.85 ± 0.16	68.84 ± 0.15	60.39 ± 0.14
$\Delta H_{(MM+solv)}$	−43.46 ± 0.11	−26.75 ± 0.17	−46.14 ± 0.10	−42.77 ± 0.12
$-T\Delta S_{tot}$	27.58 ± 0.56	24.39 ± 0.61	28.97 ± 0.57	27.03 ± 0.50
$\Delta G_{MM-PBSA}$	−15.88 ± 0.57	−2.36 ± 0.63	−17.17 ± 0.58	−15.74 ± 0.51
$\Delta\Delta G_{MM-PBSA}$	13.52		1.43	
K_i (nM)	0.0027	190809	0.00031	0.0034
$\Delta\Delta G_{TI}$	—		1.824 ± 5.396[a]	
ΔG_{exp}	−15.51	—	−16.12	—
$K_{i\ exp}$ (nM)[b]	0.005	—	0.0018	—

[a]TI calculations for **3c**−HIV-1 PR have been performed for 1 ns for each λ. [b]Experimental K_i values have been taken from refs 18a (**26** complex) and 18b (**3c** complex).

Energetic Analysis. To estimate the energetic contributions of binding in a reliable and detailed fashion, the MM−PBSA and TI methods have been applied to all complexes, and the results are summarized in Table 3. The binding energy calculations rationalized our previous observations as the four drugs presented adequate binding to the WT form of HIV-1 PR. The loss in binding energy upon I50V mutation for each complex has been predicted by MM−PBSA and TI, in agreement with the experimental results. Specifically, the deviation between experimental and predicted values lies within 7 kcal mol^{-1} for MM−PBSA and 1 kcal mol^{-1} for TI calculations. It is important to mention that even though MM−PBSA is a fast method that predicts the qualitative direction of ΔG upon mutation in each case, it is not that accurate in estimating absolute binding energies. The more costly and rigorous TI methodology, however, provides precise results in striking agreement with the experiments. We note that the standard deviations given for the TI calculations in Table 3, significantly overestimate (by at least a factor of 10) the numerical uncertainty of TI, but not necessarily the uncertainty of the calculation. That is, for each individual window, the correct $\partial V/\partial\lambda$ average is known much more precisely than the $\approx \pm 5$ kcal mol^{-1} suggests, probably more to within <0.1 kcal mol^{-1}. However, this would only be a small part of the actual error for the binding free energy ΔG, since that also includes sampling problems in each window, errors in the numerical integration, and several other deficiencies of the MM model, all of which can be much larger. Therefore, we report the RMS fluctuations for TI instead of calculating correct uncertainty estimates for each window that might be more misleading. Free energy plots for each step of the four TI computations are shown in Figure S6 of the Supporting Information.

Energy decomposition to individual contributions revealed that van der Waals and electrostatics act most favorably toward binding for all complexes. The nonpolar contribution to solvation further contributes to the total binding energy. Similar observations have been concluded in several previous studies of our group, involving a multitude of HIV-1 PR inhibitors.[58,60,61] Interestingly, it was observed that mutation I50V resulted in the decrease of the enthalpy after a significant change in the van der Waals contacts. More specifically, it was observed that the mutation affected mostly indinavir's binding into HIV-1 PR compared to other drugs, due to significant loss in van der Waals contacts, unfavorable electrostatics, and entropy change in the I50V complex. This resulted in an 11 kcal mol^{-1} energy difference between indinavir complexes that greatly diminished the drug's inhibitory potency. Importantly, the change in the entropy between the WT and mutated forms of the other drug complexes was negligible, thus implying that the increase in total binding energy upon mutation arises mostly from changes in enthalpy.

Evaluation of Two Novel Compounds As Promising Protease Inhibitors. The predictive ability of the combined MM−PBSA and TI methodologies motivated us to test the efficacy of two recently proposed anti-HIV compounds, **3c** and **26**. Conformational analysis of the WT and I50V-PR complexes with these compounds revealed that even though RMSD values for HIV-1 PR converged for all systems, they were noticeably more pronounced in the **26**-PR complexes (Figure S2 of the Supporting Information). Moreover, compound **3c** was stable in both forms of the protease, and while **26** was also stable in WT, it was significantly mobile in I50V, as depicted in Figure S3 of the Supporting Information. Similar observations arise from the conformational changes and fluctuations of the flaps that indicate an increased mobility, which resulted in several structural changes of the **26**−(I50V) PR flaps (Figures 2 and 3). The structural analysis suggested that both **3c**−HIV-1 PR complexes present conformational features that may accompany effective binding, whereas **26** induces structural changes to the I50V form of the protease that may result in reduced potency.

Hydrogen-bonding analysis further supported the above observations, as it was shown that both compounds were stabilized in the binding cavity of WT HIV-1 PR via extended HB networks (Tables 1 and 2, and Figures S6, S7, S12, and S13 of the Supporting Information). Similar to the marketed PIs, compound **3c** in I50V presented reduced (mostly flap−flap, and with Asp29′/30/30′) interactions compared to the WT, while in **26**, the reduction in HBs was more profound.

Additional MM−PBSA calculations verified the high inhibitory potency of both compounds against WT PR ($\Delta G_{MM-PBSA/\mathbf{3c}\text{-WT}} = -17.2$ kcal mol^{-1} and $\Delta G_{MM-PBSA/\mathbf{26}\text{-WT}}$

= −15.9 kcal mol^{-1}), in agreement with the experimental results (Table 4). Interestingly, while the potency of **26** was drastically reduced upon mutation, the efficacy of compound **3c** was only slightly affected by the mutation ($\Delta G_{MM-PBSA/3c\text{-}I50V}$ = −15.7 kcal mol^{-1} vs $\Delta G_{MM-PBSA/26\text{-}I50V}$ = −2.4 kcal mol^{-1}). Similarly to the other systems, the **3c** complex displayed lower electrostatic and van der Waals contributions in the I50V form than in the WT form, but it retained its potency for I50V mostly from a substantial gain in the electrostatic contribution to the solvation energy (ΔG_{PB}). The MM−PBSA results motivated us further to perform TI calculations for the **3c**-PR complexes, in order to estimate more accurately the relative energy difference between the WT and the I50V forms. The free energy curves are presented in Figure S6 of the Supporting Information. The loss in binding energy upon mutation was predicted to be $\Delta\Delta G_{TI,3c}$ = 1.8 kcal mol^{-1}, which is in agreement with the MM−PBSA calculations and also with the relative changes in binding energy for the four marketed drugs. These results clearly suggest that compound **3c** may be a very promising PI, against which the I50V mutation would provide only low resistance.

CONCLUSIONS

A systematic approach on the mechanism of the I50V drug resistance-associated mutation in HIV-1 PR has been attempted by means of molecular dynamics (MD), molecular mechanics Poisson−Boltzmann surface area (MM−PBSA), and thermodynamic integration (TI) computational methodologies. The conformational features and binding modes of four marketed, potent protease inhibitors, darunavir, amprenavir, indinavir, and saquinavir, have been compared between wild-type (WT) and I50V mutated forms of the protease to elucidate the mechanism of resistance due to the flap mutation. Conformational analysis on WT and mutated complexes with PIs revealed that the WT structures are more stable compared to the mutated ones, with the only exception of amprenavir complexes that appear equally flexible in both forms of the protease. Interestingly, both WT and I50V systems induced a closed conformation to the flaps in the presence of any inhibitor, thus suggesting that a closed structure does not necessarily imply efficient binding. This is in accordance with our previous observations regarding a fullerene analog that displayed poor binding to HIV-1 PR.[58] Despite the relative proximity of the flaps in all complexes, it was shown that there is a great difference in flap flexibility between WT and mutated forms: the flaps in most I50V complexes appear increasingly mobile compared to the WT. This is due to the stabilization of the flap tips of the WT proteases via interflap and water-mediated hydrogen bonds that are considered of major importance toward effective binding. However, these interactions are significantly diminished in the I50V complexes. Hydrogen-bonding analysis showed that the drugs were stabilized inside all complexes (WT and I50V) with significant interactions, primarily involving residues at the active site, such as the side chain of Asp25/25′ and the backbone atoms of Asp29/29′/30/30′. Importantly, similar observations regarding flap flexibility, as well as flap−flap and HB interactions, were derived from a recent study of saquinavir complexes in WT and 7 singly mutated PR strains: it was shown that the low flexibility of the flaps along with the preservation (upon mutations) of drug interactions with active site and flap residues are necessary for effective saquinavir binding.[59] MM−PBSA and more rigorous TI calculations verified the experimental results and implicated that the loss in binding energy is mostly enthalpically driven. The change in van der Waals interactions has been identified as the major component of the binding energy difference between all WT and mutated complexes. Finally, we selected two potent compounds that have been recently synthesized by Ghosh et al. as very promising PIs.[29,30] They have been designed to maximize the interactions into the binding cavity of WT HIV-1 PR and present significant potency. MM−PBSA calculations verified their excellent inhibitory effects in the WT, as the predicted values ($\Delta G_{MM-PBSA,26}$ = −15.9 kcal mol^{-1} and $\Delta G_{MM-PBSA,3c}$ = −17.2 kcal mol^{-1}) were in agreement with the experimental results ($\Delta G_{exp,26}$ = −15.5 kcal mol^{-1} and $\Delta G_{exp,3c}$ = −16.1 kcal mol^{-1}). Furthermore, TI calculations showed that the complex with compound **3c** displayed a loss in binding energy of 1.8 kcal mol^{-1} upon mutation, thus being comparable to the marketed drugs. Contrary to the other inhibitors, **3c**−HIV-1 PR presents a favorable change in the polar contribution to the solvation energy upon mutation. These results significantly strengthen the possibility of **3c** to function as a very effective protease inhibitor.

ASSOCIATED CONTENT

Supporting Information

Six additional figures showing (1) the alchemical transformation from Ile to Val for TI calculations, (2) RMSD plots for inhibitor-bound and apo forms of HIV-1 PR, (3) RMSD plots for the inhibitors, (4) Flap−flap distances for all complexes, (5) representative drug structures after clustering, and (6) free energy plots for TI calculations. Thirteen additional tables showing (1) λ values and weights used in TI calculations and (2−13) Flap−flap and inhibitor−HIV-1 PR HB interactions for HIV-1 PR complexes. This material is available free of charge via the Internet at http://pubs.acs.org.

AUTHOR INFORMATION

Corresponding Author

*G.L.: e-mail, gleonis@eie.gr. M.G.P.: e-mail, mpapad@eie.gr.

Notes

The authors declare no competing financial interest.

ACKNOWLEDGMENTS

This work was supported in part by the European Commission for the FP7-REGPOT-2009-1 Project 'ARCADE' (Grant 245866) and by the Project 'NanoPUZZLES' (Grant NMP-SL-2012-309837).

REFERENCES

(1) Wlodawer, A.; Vondrasek, J. Inhibitors of HIV-1 protease: A major success of structure-assisted drug design. *Annu. Rev. Biophys. Biomol. Struct.* **1998**, *27*, 249−284.

(2) Navia, M. A.; Fitzgerald, P. M.; McKeever, B. M.; Leu, C. T.; Heimbach, J. C.; Herber, W. K.; Sigal, I. S.; Darke, P. L.; Springer, J. P. Three-dimensional structure of aspartyl protease from human immunodeficiency virus HIV-1. *Nature* **1989**, *337*, 615−620.

(3) Brik, A.; Wong, C. H. HIV-1 protease: Mechanism and drug discovery. *Org. Biomol. Chem.* **2003**, *1*, 5−14.

(4) Miller, M.; Jaskolski, M.; Rao, J. K.; Leis, J.; Wlodawer, A. Crystal structure of a retroviral protease proves relationship to aspartic protease family. *Nature* **1989**, *337*, 576−579.

(5) Nicholson, L. K.; Yamazaki, T.; Torchia, D. A.; Grzesiek, S.; Bax, A.; Stahl, S. J.; Kaufman, J. D.; Wingfield, P. T.; Lam, P. Y.; Jadhav, P. K.; Hodge, C. N.; Domaille, P. J.; Chang, C.-H. Flexibility and function in HIV-1 protease. *Nat. Struct. Biol.* **1995**, *2*, 274−280.

(6) Freedberg, D. I.; Ishima, R.; Jacob, J.; Wang, Y. X.; Kustanovich, I.; Louis, J. M.; Torchia, D. A. Rapid structural fluctuations of the free HIV protease flaps in solution: Relationship to crystal structures and comparison with predictions of dynamics calculations. *Protein Sci.* **2002**, *11*, 221−232.
(7) Lapatto, R.; Blundell, T.; Hemmings, A.; Overington, J.; Wilderspin, A.; Wood, S.; Merson, J. R.; Whittle, P. J.; Danley, D. E.; Geoghegan, K. F.; Hawrylik, S. J.; Lee, S. E.; Scheld, K. G.; Hobart, P. M. X-ray analysis of HIV-1 proteinase at 2.7 A resolution confirms structural homology among retroviral enzymes. *Nature* **1989**, *342*, 299−302.
(8) Hornak, V.; Okur, A.; Rizzo, R. C.; Simmerling, C. HIV-1 protease flaps spontaneously open and reclose in molecular dynamics simulations. *Proc. Natl. Acad. Sci. U.S.A.* **2006**, *103*, 915−920.
(9) Hornak, V.; Okur, A.; Rizzo, R. C.; Simmerling, C. HIV-1 protease flaps spontaneously close to the correct structure in simulations following manual placement of an inhibitor into the open state. *J. Am. Chem. Soc.* **2006**, *128*, 2812−2813.
(10) Vondrasek, J.; Wlodawer, A. HIVdb: A database of the structures of human immunodeficiency virus protease. *Proteins* **2002**, *49*, 429−431.
(11) Hyland, L. J.; Tomaszek, T. A., Jr.; Meek, T. D. Human immunodeficiency virus-1 protease. 2. Use of pH rate studies and solvent kinetic isotope effects to elucidate details of chemical mechanism. *Biochemistry* **1991**, *30*, 8454−8463.
(12) Pietrucci, F.; Marinelli, F.; Carloni, P.; Laio, A. Substrate binding mechanism of HIV-1 protease from explicit-solvent atomistic simulations. *J. Am. Chem. Soc.* **2009**, *131*, 11811−11818.
(13) Piana, S.; Sebastiani, D.; Carloni, P.; Parrinello, M. Ab initio molecular dynamics-based assignment of the protonation state of pepstatin A/HIV-1 protease cleavage site. *J. Am. Chem. Soc.* **2001**, *123*, 8730−8737.
(14) Hou, T.; McLaughlin, W. A.; Wang, W. Evaluating the potency of HIV-1 protease drugs to combat resistance. *Proteins* **2008**, *71*, 1163−1174.
(15) Zhu, Z.; Schuster, D. I.; Tuckerman, M. E. Molecular dynamics study of the connection between flap closing and binding of fullerene-based inhibitors of the HIV-1 protease. *Biochemistry* **2003**, *42*, 1326−1333.
(16) Ghosh, A. K. *Aspartic Acid Proteases as Therapeutic Targets*. John Wiley and Sons: Hoboken, NJ, 2011.
(17) Wlodawer, A.; Erickson, J. W. Structure-based inhibitors of HIV-1 protease. *Annu. Rev. Biochem.* **1993**, *62*, 543−585.
(18) Barbaro, G.; Scozzafava, A.; Mastrolorenzo, A.; Supuran, C. T. Highly active antiretroviral therapy: Current state of the art, new agents and their pharmacological interactions useful for improving therapeutic outcome. *Curr. Pharm. Des.* **2005**, *11*, 1805−1843.
(19) Coffin, J. M. HIV population dynamics in vivo: Implications for genetic variation, pathogenesis, and therapy. *Science* **1995**, *267*, 483−489.
(20) Gu, Z.; Gao, Q.; Fang, H.; Salomon, H.; Parniak, M. A.; Goldberg, E.; Cameron, J.; Wainberg, M. A. Identification of a mutation at codon 65 in the IKKK motif of reverse transcriptase that encodes human immunodeficiency virus resistance to 2′,3′-dideoxycytidine and 2′,3′-dideoxy-3′-thiacytidine. *Antimicrob. Agents Chemother.* **1994**, *38*, 275−281.
(21) Baldwin, E. T.; Bhat, T. N.; Liu, B.; Pattabiraman, N.; Erickson, J. W. Structural basis of drug resistance for the V82A mutant of HIV-1 proteinase. *Nat. Struct. Biol.* **1995**, *2*, 244−249.
(22) Johnson, V. A.; Brun-Vezinet, F.; Clotet, B.; Gunthard, H. F.; Kuritzkes, D. R.; Pillay, D.; Schapiro, J. M.; Richman, D. D. Update of the drug resistance mutations in HIV-1: December 2009. *Topics in HIV Medicine* **2009**, *17*, 138−145.
(23) Johnson, V. A.; Brun-Vezinet, F.; Clotet, B.; Conway, B.; D'Aquila, R. T.; Demeter, L. M.; Kuritzkes, D. R.; Pillay, D.; Schapiro, J. M.; Telenti, A.; Richman, D. D. Update of the drug resistance mutations in HIV-1: 2004. *Topics in HIV Medicine* **2004**, *12*, 119−124.
(24) Cai, Y.; Schiffer, C. A. Decomposing the energetic impact of drug resistant mutations in HIV-1 protease on binding DRV. *J. Chem. Theory Comput.* **2010**, *6*, 1358−1368.
(25) Hou, T.; Yu, R. Molecular dynamics and free energy studies on the wild-type and double mutant HIV-1 protease complexed with amprenavir and two amprenavir-related inhibitors: Mechanism for binding and drug resistance. *J. Med. Chem.* **2007**, *50*, 1177−1188.
(26) Ode, H.; Neya, S.; Hata, M.; Sugiura, W.; Hoshino, T. Computational simulations of HIV-1 proteases−multi-drug resistance due to nonactive site mutation L90M. *J. Am. Chem. Soc.* **2006**, *128*, 7887−7895.
(27) Meher, B. R.; Wang, Y. Interaction of I50V mutant and I50L/A71V double mutant HIV-protease with inhibitor TMC114 (darunavir): Molecular dynamics simulation and binding free energy studies. *J. Phys. Chem. B* **2012**, *116*, 1884−1900.
(28) RCSB Protein Data Bank. http://www.rcsb.org/pdb/home/home.do (accessed March 2013).
(29) Ghosh, A. K.; Chapsal, B. D.; Parham, G. L.; Steffey, M.; Agniswamy, J.; Wang, Y. F.; Amano, M.; Weber, I. T.; Mitsuya, H. Design of HIV-1 protease inhibitors with C3-substituted hexahydrocyclopentafuranyl urethanes as P2-ligands: Synthesis, biological evaluation, and protein-ligand X-ray crystal structure. *J. Med. Chem.* **2011**, *54*, 5890−5901.
(30) Ghosh, A. K.; Chapsal, B. D.; Steffey, M.; Agniswamy, J.; Wang, Y. F.; Amano, M.; Weber, I. T.; Mitsuya, H. Substituent effects on P2-cyclopentyltetrahydrofuranyl urethanes: Design, synthesis, and X-ray studies of potent HIV-1 protease inhibitors. *Bioorg. Med. Chem. Lett.* **2012**, *22*, 2308−2311.
(31) Tie, Y.; Boross, P. I.; Wang, Y. F.; Gaddis, L.; Hussain, A. K.; Leshchenko, S.; Ghosh, A. K.; Louis, J. M.; Harrison, R. W.; Weber, I. T. High resolution crystal structures of HIV-1 protease with a potent non-peptide inhibitor (UIC-94017) active against multi-drug-resistant clinical strains. *J. Mol. Biol.* **2004**, *338*, 341−352.
(32) Shen, C. H.; Wang, Y. F.; Kovalevsky, A. Y.; Harrison, R. W.; Weber, I. T. Amprenavir complexes with HIV-1 protease and its drug-resistant mutants altering hydrophobic clusters. *FEBS J.* **2010**, *277*, 3699−3714.
(33) Mahalingam, B.; Wang, Y. F.; Boross, P. I.; Tozser, J.; Louis, J. M.; Harrison, R. W.; Weber, I. T. Crystal structures of HIV protease V82A and L90M mutants reveal changes in the indinavir-binding site. *Eur. J. Biochem.* **2004**, *271*, 1516−1524.
(34) Liu, F.; Boross, P. I.; Wang, Y. F.; Tozser, J.; Louis, J. M.; Harrison, R. W.; Weber, I. T. Kinetic, stability, and structural changes in high-resolution crystal structures of HIV-1 protease with drug-resistant mutations L24I, I50V, and G73S. *J. Mol. Biol.* **2005**, *354*, 789−800.
(35) Tie, Y.; Kovalevsky, A. Y.; Boross, P.; Wang, Y. F.; Ghosh, A. K.; Tozser, J.; Harrison, R. W.; Weber, I. T. Atomic resolution crystal structures of HIV-1 protease and mutants V82A and I84V with saquinavir. *Proteins* **2007**, *67*, 232−242.
(36) Salomon-Ferrer, R.; Case, D. A.; Walker, R. C. An overview of the Amber biomolecular simulation package. *Wiley Interdiscip. Rev.: Comput. Mol. Sci.* **2012**, DOI: 10.1002/wcms.1121.
(37) Case, D. A.; Cheatham, T. E., 3rd; Darden, T.; Gohlke, H.; Luo, R.; Merz, K. M., Jr.; Onufriev, A.; Simmerling, C.; Wang, B.; Woods, R. J. The Amber biomolecular simulation programs. *J. Comput. Chem.* **2005**, *26*, 1668−1688.
(38) Case, D. A.; Darden T.; Cheatham, T. E., III, Simmerling, C. L.; Wang, J.; Duke, R. E.; Luo, R.; Walker, R. C.; Zhang, W.; Merz, K. M.; Roberts, B. P.; Wang, B.; Hayik, S.; Roitberg, A.; Seabra, G.; Kolossvai, I.; Wong, K. F.; Paesani, F.; Vanicek, J.; Liu, J.; Wu, X.; Brozell, S. R.; Steinbrecher, T.; Gohlke, H.; Cai, Q.; Ye, X.; Wang, J.; Hsieh, M.-J.; Cui, G.; Roe, D. R.; Mathews, D. H.; Seetin, M. G.; Sagui, C.; Babin, V.; Luchko, T.; Gusarov, S.; Kovalenko, A.; Kollman, P. A. *AMBER 11*; University of California: San Francisco, 2010.
(39) Hornak, V.; Abel, R.; Okur, A.; Strockbine, B.; Roitberg, A.; Simmerling, C. Comparison of multiple Amber force fields and development of improved protein backbone parameters. *Proteins* **2006**, *65*, 712−725.

(40) Word, J. M.; Lovell, S. C.; Richardson, J. S.; Richardson, D. C. Asparagine and glutamine: Using hydrogen atom contacts in the choice of side-chain amide orientation. *J. Mol. Biol.* **1999**, *285*, 1735−1747.
(41) Frisch, M. J.; Trucks, G. W.; Schlegel, H. B.; Scuseria, G. E.; Robb, M. A.; Cheeseman, J. R.; Scalmani, G.; Barone, V.; Mennucci, B.; Petersson, G. A.; Nakatsuji, H.; Caricato, M.; Li, X.; Hratchian, H. P.; Izmaylov, A. F.; Bloino, J.; Zheng, G.; Sonnenberg, J. L.; Hada, M.; Ehara, M.; Toyota, K.; Fukuda, R.; Hasegawa, J.; Ishida, M.; Nakajima, T.; Honda, Y.; Kitao, O.; Nakai, H.; Vreven, T.; Montgomery, J. A., Jr.; Peralta, J. E.; Ogliaro, F.; Bearpark, M.; Heyd, J. J.; Brothers, E.; Kudin, K. N.; Staroverov, V. N.; Kobayashi, R.; Normand, J.; Raghavachari, K.; Rendell, A.; Burant, J. C.; Iyengar, S. S.; Tomasi, J.; Cossi, M.; Rega, N.; Millam, N. J.; Klene, M.; Knox, J. E.; Cross, J. B.; Bakken, V.; Adamo, C.; Jaramillo, J.; Gomperts, R.; Stratmann, R. E.; Yazyev, O.; Austin, A. J.; Cammi, R.; Pomelli, C.; Ochterski, J. W.; Martin, R. L.; Morokuma, K.; Zakrzewski, V. G.; Voth, G. A.; Salvador, P.; Dannenberg, J. J.; Dapprich, S.; Daniels, A. D.; Farkas, Ö.; Foresman, J. B.; Ortiz, J. V.; Cioslowski, J.; Fox, D. J. *Gaussian 09*; Gaussian, Inc.: Wallingford, CT, 2009.
(42) Wang, J.; Wolf, R. M.; Caldwell, J. W.; Kollman, P. A.; Case, D. A. Development and testing of a general amber force field. *J. Comput. Chem.* **2004**, *25*, 1157−1174.
(43) Jorgensen, W. L.; Chandrasekhar, J.; Madura, J. D.; Impey, R. W.; Klein, M. L. Comparison of simple potential functions for simulating liquid water. *J. Chem. Phys.* **1983**, *79*, 926−935.
(44) Darden, T.; York, D.; Pedersen, L. Particle Mesh Ewald-an N.Log(N) method for Ewald sums in large systems. *J. Chem. Phys.* **1993**, *98*, 10089−10092.
(45) Ryckaert, J. P.; Ciccotti, G.; Berendsen, H. J. C. Numerical integration of the cartesian equations of motion of a system with constraints: Molecular dynamics of n-Alkanes. *J. Comput. Phys.* **1977**, *23*, 327−341.
(46) Izaguirre, J. A.; Catarello, D. P.; Wozniak, J. M.; Skeel, R. D. Langevin Stabilization of Molecular Dynamics. *J. Chem. Phys.* **2001**, *114*, 2090−2098.
(47) Simmerling, C.; Elber, R.; Zhang, J. Moil-view—A program for visualization of structure and dynamics of biomolecules and STO—A program for computing stochastic paths. *The Jerusalem Symposia on Quantum Chemistry and Biochemistry* **1995**, *27*, 241−265.
(48) Simonson, T.; Archontis, G.; Karplus, M. Free energy simulations come of age: Protein-ligand recognition. *Acc. Chem. Res.* **2002**, *35*, 430−437.
(49) Kollman, P. A.; Massova, I.; Reyes, C.; Kuhn, B.; Huo, S.; Chong, L.; Lee, M.; Lee, T.; Duan, Y.; Wang, W.; Donini, O.; Cieplak, P.; Srinivasan, J.; Case, D. A.; Cheatham, T. E., III Calculating structures and free energies of complex molecules: Combining molecular mechanics and continuum models. *Acc. Chem. Res.* **2000**, *33*, 889−897.
(50) Gohlke, H.; Kiel, C.; Case, D. A. Insights into protein-protein binding by binding free energy calculation and free energy decomposition for the Ras-Raf and Ras-RalGDS complexes. *J. Mol. Biol.* **2003**, *330*, 891−913.
(51) Wang, W.; Kollman, P. A. Computational study of protein specificity: The molecular basis of HIV-1 protease drug resistance. *Proc. Natl. Acad. Sci. U.S.A.* **2001**, *98*, 14937−14942.
(52) Xu, Y.; Wang, R. A computational analysis of the binding affinities of FKBP12 inhibitors using the MM-PB/SA method. *Proteins* **2006**, *64*, 1058−1068.
(53) Honig, B.; Nicholls, A. Classical electrostatics in biology and chemistry. *Science* **1995**, *268*, 1144−1149.
(54) Weiser, J.; Shenkin, P. S.; Still, W. C. Approximate atomic surfaces from linear combinations of pairwise overlaps (LCPO). *J. Comput. Chem.* **1999**, *20*, 217−230.
(55) Hou, T.; Wang, J.; Li, Y.; Wang, W. Assessing the performance of the MM/PBSA and MM/GBSA methods. 1. The accuracy of binding free energy calculations based on molecular dynamics simulations. *J. Chem. Inf. Model.* **2011**, *51*, 69−82.
(56) Kirkwood, J. G. Statistical Mechanics of Fluid Mixtures. *J. Chem. Phys.* **1935**, *3*, 300−313.
(57) Steinbrecher, T.; Mobley, D. L.; Case, D. A. Nonlinear scaling schemes for Lennard-Jones interactions in free energy calculations. *J. Chem. Phys.* **2007**, *127*, 214108−214121.
(58) Leonis, G.; Czyznikowska, Z.; Megariotis, G.; Reis, H.; Papadopoulos, M. G. Computational studies of darunavir into HIV-1 protease and DMPC bilayer: Necessary conditions for effective binding and the role of the flaps. *J. Chem. Inf. Model.* **2012**, *52*, 1542−1558.
(59) Tzoupis, H.; Leonis, G.; Mavromoustakos, T. M.; Papadopoulos, M. G. A comparative molecular dynamics, MM−PBSA and thermodynamic integration study of saquinavir complexes with wild-type HIV-1 PR and L10I, G48V, L63P, A71V, G73S, V82A and I84V single mutants. *J. Chem. Theory Comput.* **2013**, *9*, 1754−1764.
(60) Tzoupis, H.; Leonis, G.; Megariotis, G.; Supuran, C. T.; Mavromoustakos, T.; Papadopoulos, M. G. Dual inhibitors for aspartic proteases HIV-1 PR and renin: Advancements in AIDS-hypertension-diabetes linkage via molecular dynamics, inhibition assays, and binding free energy calculations. *J. Med. Chem.* **2012**, *55*, 5784−5796.
(61) Tzoupis, H.; Leonis, G.; Durdagi, S.; Mouchlis, V.; Mavromoustakos, T.; Papadopoulos, M. G. Binding of novel fullerene inhibitors to HIV-1 protease: Insight through molecular dynamics and molecular mechanics Poisson-Boltzmann surface area calculations. *J. Comput.-Aided Mol. Des.* **2011**, *25*, 959−976.
(62) Liu, F.; Kovalevsky, A. Y.; Tie, Y.; Ghosh, A. K.; Harrison, R. W.; Weber, I. T. Effect of flap mutations on structure of HIV-1 protease and inhibition by saquinavir and darunavir. *J. Mol. Biol.* **2008**, *381*, 102−115.